

1-20-2007

Mosaicking with Cosmic Microwave Background Interferometers

Emory F. Bunn

University of Richmond, ebunn@richmond.edu

Martin White

Follow this and additional works at: <http://scholarship.richmond.edu/physics-faculty-publications>Part of the [Cosmology, Relativity, and Gravity Commons](#), and the [Instrumentation Commons](#)

Recommended Citation

Bunn, Emory F., and Martin White. "Mosaicking with Cosmic Microwave Background Interferometers." *The Astrophysical Journal* 655, no. 1 (January 20, 2007): 21-29. doi:10.1086/509867.

This Article is brought to you for free and open access by the Physics at UR Scholarship Repository. It has been accepted for inclusion in Physics Faculty Publications by an authorized administrator of UR Scholarship Repository. For more information, please contact scholarshiprepository@richmond.edu.

MOSAICKING WITH COSMIC MICROWAVE BACKGROUND INTERFEROMETERS

EMORY F. BUNN

Physics Department, University of Richmond, Richmond, VA

AND

MARTIN WHITE

Departments of Physics and Astronomy, University of California, Berkeley, CA

Received 2006 June 19; accepted 2006 September 22

ABSTRACT

Measurements of cosmic microwave background (CMB) anisotropies by interferometers offer several advantages over single-dish observations. The formalism for analyzing interferometer CMB data is well developed in the flat-sky approximation, which is valid for small fields of view. As the area of sky is increased to obtain finer spectral resolution, this approximation needs to be relaxed. We extend the formalism for CMB interferometry, including both temperature and polarization, to mosaics of observations covering arbitrarily large areas of the sky, with each individual pointing lying within the flat-sky approximation. We present a method for computing the correlation between visibilities with arbitrary pointing centers and baselines and illustrate the effects of sky curvature on the ℓ -space resolution that can be obtained from a mosaic.

Subject headings: cosmic microwave background — techniques: interferometric

1. INTRODUCTION

The study of anisotropies in the cosmic microwave background (CMB) radiation has revolutionized cosmology. Key to this revolution have been coupled advances in theory, data analysis, and instrumentation. In particular, the design of experiments with exquisite systematic error control has been crucial for progress in the field. Interferometers offer several advantages in this respect, with simple optics, instantaneous differencing of sky signals without scanning, and no differencing of detectors. The shape of the beam can be well understood, and the measurement is done directly in Fourier space where the theory most naturally lives.

Pioneering attempts to detect CMB anisotropy with interferometers were made by Martin & Partridge (1988) and Subrahmanyam et al. (1993). Several groups have successfully detected primary CMB anisotropies (O’Sullivan et al. 1995; Baker et al. 1999; Halverson et al. 2002; Pearson et al. 2003; Taylor et al. 2003) and polarization (Readhead et al. 2004; Leitch et al. 2005), using interferometers. The formalism for analyzing CMB data from interferometers has been developed by Hobson et al. (1995), Hobson & Magueijo (1996), White et al. (1999), Hobson & Maisinger (2002), and Myers et al. (2003), as well as in the experimental papers cited above. Park et al. (2003) and Park & Ng (2004) examined interferometric polarimetry.

In the Fraunhofer limit an interferometer measures the Fourier transform of the sky multiplied by the primary beam. The primary beam determines the instantaneous field of view of the instrument, and its Fourier transform is simply the autocorrelation of the Fourier transform of the point response of the receiver to an electric field. The angular scale probed by any pair of telescopes being correlated is determined by their spacing in units of the observational wavelength.¹ The range of scales probed by the interferometer is then determined by the spacing of the elements, while the resolution in spatial wavenumber is determined by the area of sky surveyed. By “mosaicking” several smaller patches together, the resolution

in spatial wavenumber can be increased, although the range of spatial scales remains fixed by the geometry of the interferometer elements (Ekers & Rots 1979; Cornwell 1988; Cornwell et al. 1993; Holdaway 1999).

In most cases it has been assumed that the field of view is small, so that one can use the “small-angle” or “flat-sky” approximation, but this assumption will need to be relaxed in future experiments. The CMB angular power spectrum has relatively narrow features in spatial wavenumber (i.e., multipole ℓ), so future experiments will aim for fine Fourier-space resolution, requiring a survey of a large area of sky. On the other hand, since these features are found at relatively small angular scales, fine angular resolution is also required. In an interferometric experiment, these goals will presumably be achieved by observing a mosaic of many pointings with small individual fields of view. The purpose of this paper is to extend the formalism presented in the above papers to the case in which each individual pointing of the interferometer is still within the flat-sky approximation but by mosaicking many pointings together a significant area of sky is surveyed. Our extension allows one to see how large an error is being made in assuming the flat-sky approximation and shows how corrections can be systematically incorporated.

The central idea of this paper is the following. The key ingredient in analyzing a mosaic of interferometer pointings is the set of two-point visibility correlations. For each pair of pointings we can calculate the correlations in a spherical coordinate system that places both pointing centers on the equator. If each pointing has a small field of view, then we can approximate the sphere by a cylinder in the vicinity of the equator, allowing the use of Fourier analysis, rather than a more cumbersome expansion in spherical harmonics. With this formalism, correlations can be found for pointings with centers separated by arbitrarily large angles. Knowledge of these correlations is essential if we wish to achieve fine ℓ -space resolution.

The outline of this paper is as follows. We begin in § 2 by reminding the reader of some basic results in the flat-sky limit. We then show how this can be extended using a cylindrical projection in § 3 and make contact with the exact spherical harmonic

¹ We assume monochromatic radiation throughout; the generalization to a specified frequency band is straightforward.

treatment in § 4. Section 5 extends our results to include polarization, and we conclude in § 6.

2. FLAT-SKY LIMIT

We begin by considering the flat-sky limit and focusing on temperature anisotropies. Thus, our interferometer is measuring a scalar field, $T(\mathbf{x})$, defined on the two-dimensional plane. In this limit the fundamental observable, a visibility, can be written as

$$V(\mathbf{u}) = \frac{\partial B_\nu}{\partial T} \int d^2\mathbf{x} \Delta T(\mathbf{x}) A(\mathbf{x}) e^{2\pi i \mathbf{u} \cdot \mathbf{x}}, \quad (1)$$

where $\partial B_\nu / \partial T$ converts from temperature to intensity units and $A(\mathbf{x})$ is the primary beam (typically normalized to unity at the peak). From now on we neglect the flux-temperature conversion factors and write T for ΔT .

For Gaussian fluctuations, such as the primary CMB anisotropies, we need to compute the visibility correlation matrix:

$$\mathcal{V}_{ij} \equiv \langle V(\mathbf{u}_i) V^*(\mathbf{u}_j) \rangle, \quad (2)$$

where \mathbf{u}_i and \mathbf{u}_j represent the baselines to be correlated and $\langle \dots \rangle$ represents an ensemble average. This can be related to the usual temperature correlation function,

$$\langle T(\mathbf{n}_i) T(\mathbf{n}_j) \rangle = \frac{1}{4\pi} \sum_{\ell=2}^{\infty} (2\ell + 1) C_\ell P_\ell(\mathbf{n}_i \cdot \mathbf{n}_j) \quad (3)$$

for temperatures measured in directions \mathbf{n}_i and \mathbf{n}_j , where C_ℓ are the multipole moments. In our flat-sky limit, for a single patch (e.g., White et al. 1999)

$$\mathcal{V}_{ij} \propto \int d^2\mathbf{w} S(\mathbf{w}) \tilde{A}^*(2\pi(\mathbf{w} + \mathbf{u}_i)) \tilde{A}(2\pi(\mathbf{w} + \mathbf{u}_j)), \quad (4)$$

where the angular power spectrum $S(u)$ is defined by

$$(2\pi)^2 u^2 S(u) \simeq \ell(\ell + 1) C_\ell \text{ for } \ell = 2\pi u \quad (5)$$

and \tilde{A} is the Fourier transform of the antenna pattern,

$$\tilde{A}(\mathbf{k}) = (2\pi)^{-2} \int d^2\mathbf{x} A(\mathbf{x}) e^{-i\mathbf{k} \cdot \mathbf{x}}. \quad (6)$$

The extension to multiple different patches, each with its own pointing center \mathcal{P} , merely inserts a phase factor,

$$\mathcal{V}_{ij}^{\mathcal{P}_1 \mathcal{P}_2} \propto \int [d^2\mathbf{w} S(\mathbf{w}) \tilde{A}^*(2\pi(\mathbf{w} + \mathbf{u}_i)) \times \tilde{A}(2\pi(\mathbf{w} + \mathbf{u}_j)) e^{2\pi i \mathbf{w} \cdot \mathbf{D}}], \quad (7)$$

where \mathbf{D} is the separation between the pointing centers \mathcal{P}_1 and \mathcal{P}_2 . From now on we drop the superscripts on \mathcal{V}_{ij} .

The small-angle approximation made throughout this paper says that $A(\mathbf{x})$ differs significantly from zero only when $|\mathbf{x}| \ll 1$ radian. If we do not wish to make this approximation, we can replace equation (1) with (Thompson et al. 1994; Hobson & Masingier 2002)

$$V(\mathbf{u}) = \int \left\{ d^2\mathbf{x} T(\mathbf{x}) A(\mathbf{x}) \left(1 - |\mathbf{x}|^2\right)^{-1/2} \times e^{2\pi i [\mathbf{u} \cdot \mathbf{x} + w(\sqrt{1-|\mathbf{x}|^2} - 1)]} \right\}, \quad (8)$$

where w is the component of the baseline vector along the line of sight (i.e., perpendicular to the plane containing the vectors \mathbf{x} and \mathbf{u}). The visibility covariance equation (7) must be modified by replacing A with an effective antenna pattern,

$$A_{\text{eff}}(\mathbf{x}; w) = A(\mathbf{x}) \left(1 - |\mathbf{x}|^2\right)^{-1/2} e^{2\pi i w (\sqrt{1-|\mathbf{x}|^2} - 1)}. \quad (9)$$

Care must be taken in using this expression, however. When the small-angle approximation breaks down, so does the correspondence (5) between the flat-sky power spectrum S and the exact spherical harmonic power spectrum C_ℓ . In general, if the field of view is large enough that one is considering “ w -corrections” of the form (9), it is probably necessary to do a full spherical harmonic analysis, rather than one based on projecting the sky onto a plane and using Fourier transforms. For the rest of this paper we assume small fields of view and neglect w -corrections.

3. CYLINDRICAL METHOD

The flat-sky approximation above is valid only if both the field of view of an individual pointing and the separation \mathbf{D} between pointings are small. We now assume a mosaic of pointings that cover a large area, although each individual pointing observes only a small patch of sky. We therefore relax the second assumption while retaining the first.

For a statistically isotropic temperature field, we are free to use any coordinate system we like to compute the visibility correlation \mathcal{V}_{12} . In particular, we can arrange to have the two pointing centers lie on the equator of a spherical coordinate system ($\theta = \pi/2$) and be separated by an angle β . We introduce a cylindrical coordinate system, with the cylinder tangent to the sphere at the equator, denoted by $\boldsymbol{\xi} = (\phi, z)$. Since both observations sample only regions near the equator, we can pretend that the data live on the cylinder rather than on the sphere. In this approximation, it is natural to expand the temperature $T(\mathbf{x})$ in a discrete Fourier series in ϕ and a continuous Fourier transform in z :

$$T(\boldsymbol{\xi}) = \sum_m \int dn \tilde{T}_m(n) e^{i(m\phi + nz)} \quad (10)$$

with

$$\langle \tilde{T}_m(n) \tilde{T}_m^*(n') \rangle = \frac{\mathcal{P}(\sqrt{m^2 + n^2})}{(2\pi)^2} \delta_{mm'} \delta(n - n'). \quad (11)$$

The power spectrum is $\mathcal{P}(k) = (2\pi)^2 S(k/2\pi)$ with S as defined in equation (5). It is related to the spherical harmonic angular power spectrum by $\mathcal{P}(k) \simeq C_k$ for large k .

The visibility becomes

$$V(\mathcal{P}_1, \mathbf{u}_1) = (2\pi)^2 \int dn \sum_m \tilde{T}_m(n) \tilde{A}^*(2\pi(\mathbf{u}_1 + \mathbf{w})), \quad (12)$$

where the vector \mathbf{w} has coordinates $(w_\phi, w_z) = (m, n)/(2\pi)$ and

$$\tilde{A}(\mathbf{k}) = \int \frac{d^2\boldsymbol{\xi}}{(2\pi)^2} A(\boldsymbol{\xi}) e^{-i\mathbf{k} \cdot \boldsymbol{\xi}} \quad (13)$$

is the usual Fourier transform of the primary beam. Since we imagine that A is nonzero only over a small region, we can extend the integral over the entire plane.

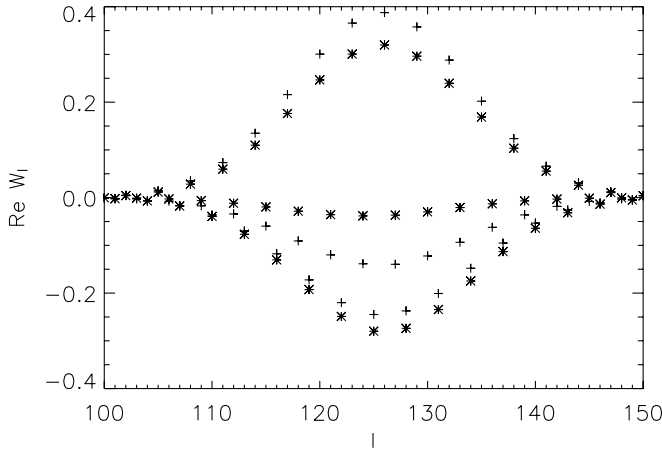


FIG. 1.—Window functions for the covariance between two interferometer pointings in both the flat and cylindrical approximations. The antenna pattern is Gaussian with beam width $\sigma = 5^\circ$. The two pointings are separated by 120° . Each visibility has a baseline of magnitude $u = 20$ pointing in the $\hat{\phi}$ -direction. The plus signs are the cylindrical approximation, and the stars are the flat approximation. For clarity, only the real parts of the window functions are shown.

The visibility for the second pointing center is analogous, except for a phase factor $e^{im\beta}$, so the correlation between two pointings becomes

$$\mathcal{V}_{12} \propto \int dn \sum_m S(w) \mathcal{W}_{12}(\mathbf{u}_1, \mathbf{u}_2, \mathbf{w}) e^{im\beta}, \quad (14)$$

where we have defined the window function,

$$\mathcal{W}_{12}(\mathbf{u}_1, \mathbf{u}_2, \mathbf{w}) \equiv \tilde{A}^*(2\pi(\mathbf{u}_1 + \mathbf{w})) \tilde{A}(2\pi(\mathbf{u}_2 + \mathbf{w})). \quad (15)$$

It is convenient to define a window function that is averaged over direction:

$$\mathcal{V}_{12} = \sum_\ell \mathcal{W}_\ell^{(12)} C_\ell. \quad (16)$$

To compute $\mathcal{W}_\ell^{(12)}$ we divide the integral and sum in equation (14) into bands with $\ell - \frac{1}{2} < 2\pi w < \ell + \frac{1}{2}$. Within each band we assume that the power spectrum is constant and remove it from the integral. We can calculate this window function in the flat-sky approximation instead of the cylindrical approximation if we like, simply by replacing the sum over m by an integral.

Figure 1 illustrates the difference between the flat and cylindrical approximations for large β . Note that the window function in this case oscillates rapidly as a function of ℓ , averaging to zero. As a result, if the power spectrum is nearly flat over the width of this window function, the correlation \mathcal{V}_{12} will be quite small due to cancellations. However, even for extremely large β the window function is not small in absolute value. For instance, the sum $\sum_\ell |\mathcal{W}_\ell^{(12)}|$ for $\beta = 120^\circ$ is 0.76 times the value for $\beta = 0$. This means that narrow ℓ -space features in the power spectrum will give rise to significant correlations even at large β ; indeed, this sort of correlation is precisely the reason that mosaicking leads to improved ℓ -space resolution.

For wide separations, \mathcal{W}_{12} differs significantly from zero, and the difference between flat and cylindrical approximations is most important when the baseline vectors \mathbf{u}_i are nearly equal in magnitude and parallel to the separation direction $\hat{\phi}$.

We can use this prescription to calculate the full visibility covariance matrix for a mosaic of many pointings. For each pair of pointings, we must transform to a coordinate system in which

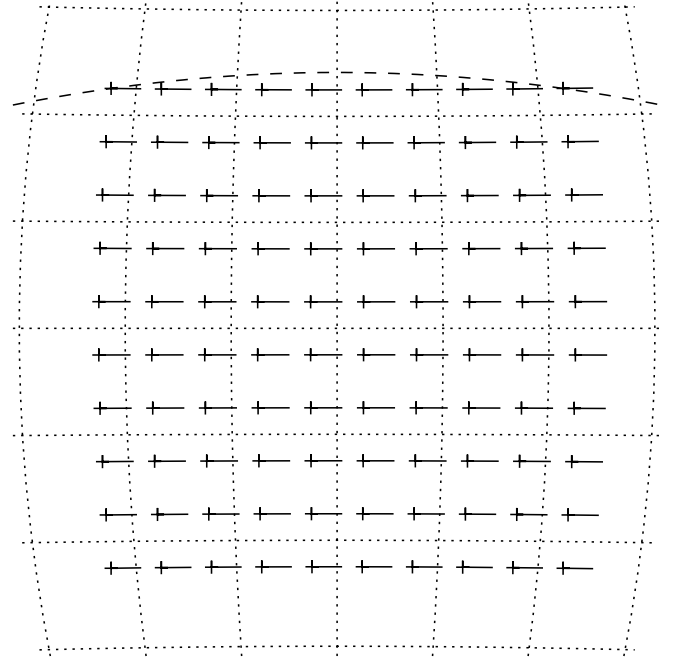


FIG. 2.—Pointing centers (*plus signs*) and baseline vectors (*horizontal bars*) for the mosaicking example described at the end of § 3. In calculating the covariance between the two visibilities at the upper corners of the grid, we must rotate to a coordinate system in which the great circle connecting them (*dashed line*) becomes the equator. Note that the two baseline vectors are not parallel in the new coordinate system.

both pointings lie on the equator. In performing this rotation, the components of the baseline vectors \mathbf{u}_i will naturally be transformed. The Appendix contains an explicit recipe for performing this rotation.

Figures 2 and 3 present a simple illustration of how mosaicking increases the ℓ -space resolution of an experiment. In each pointing, the beam pattern is a Gaussian with beam width $\sigma = 5^\circ$. We assume a 10×10 grid of pointings, separated by 5° in both θ and ϕ in a spherical coordinate system, with the center of the grid on the equator ($\theta = \pi/2$). For each pointing we consider only a single baseline $\mathbf{u} = 22\hat{\phi}$. Figure 2 shows the locations of the pointing centers and the baselines in Aitoff projection. Note that although all the baselines have identical components in the spherical coordinate system, they do not when rotated to the appropriate coordinate system for computing the covariances. As an example, to compute the covariance between the two pointings in the upper corners of the grid, we must use a coordinate system in which the great circle represented by the dashed line becomes the equator. In this coordinate system, the two baseline vectors have $\hat{\theta}$ components of opposite sign.

The visibility obtained from any single pointing provides an estimate of the power spectrum with a fairly wide window function (Fig. 3, *solid curve*). We can obtain an estimate of the power spectrum with a narrower window function by simply adding together all 100 visibilities. To find the window function for the sum, we write down the absolute square of the sum of all 100 visibilities,

$$\left\langle \left| \sum_{i=1}^{100} V_i \right|^2 \right\rangle = \sum_{i,j=1}^{100} \langle V_i V_j^* \rangle = \sum_{i,j=1}^{100} \mathcal{V}_{ij}. \quad (17)$$

The window function for the sum of all the visibilities is therefore the sum of $\mathcal{W}_l^{(ij)}$ over all visibility pairs i, j . We can compute each $\mathcal{W}_l^{(ij)}$ using the recipe described above. Specifically, for each

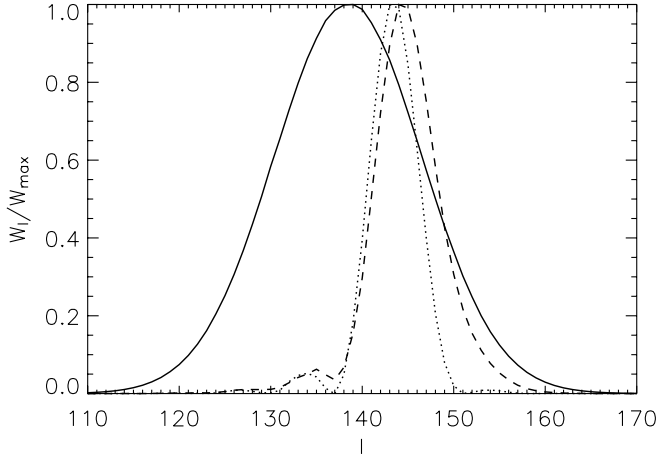


FIG. 3.—Improvement in ℓ -space resolution due to mosaicking. The solid curve is the window function for a single pointing. The dashed curve is the window function for the sum of all pointings in a 10×10 grid, after correctly accounting for baseline rotation. The dotted curve is the window function that would be obtained by incorrectly assuming a flat sky over the entire mosaic. All three window functions have arbitrary normalization.

pair of pointings, we find a rotation that brings both pointing centers to the equator, apply that rotation to the vectors \mathbf{u}_1 and \mathbf{u}_2 using the recipe in the Appendix, and apply equation (15).

The dashed curve in Figure 3 is the window function for the sum of all pointings. As expected, the ℓ -space resolution has improved. The dotted curve shows the window function obtained by incorrectly assuming that the sky is flat over the entire mosaic, that is, assuming that all of the baseline vectors illustrated in Figure 2 lie in the same plane and are parallel.

The difference between the dashed and dotted curves is almost entirely due to “baseline rotation”—the fact that, e.g., the baseline vectors at the corners of Figure 2 are not in fact parallel to each other when viewed in a coordinate system in which both lie on the equator. It makes virtually no difference whether we use the flat method (integral over m), the cylindrical method (sum over m), or an exact spherical harmonic calculation as described below in calculating each $W_\ell^{(ij)}$, as long as we get the baseline rotation right.

Of course, other linear combinations could be used instead of a simple sum of all 100 pointings, resulting in window functions with peaks in different places (within the envelope set by the single-pointing window function).

4. HARMONIC METHOD

We can also make direct contact with the usual spherical harmonic treatment in which

$$T(\hat{\mathbf{r}}) = \sum_{\ell m} a_{\ell m} Y_{\ell m}(\hat{\mathbf{r}}) \quad (18)$$

and

$$\langle a_{\ell m} a_{\ell' m'}^* \rangle = C_\ell \delta_{\ell \ell'} \delta_{m m'}. \quad (19)$$

The visibility for a single pointing is

$$V(\mathbf{u}) = \int d^2 \hat{\mathbf{r}} A(\hat{\mathbf{r}}) T(\hat{\mathbf{r}}) e^{2\pi i \mathbf{u} \cdot \hat{\mathbf{r}}} = \sum_{\ell, m} a_{\ell m} F_{\ell m}(\mathbf{u}), \quad (20)$$

where

$$F_{\ell m}(\mathbf{u}) = \int d^2 \hat{\mathbf{r}} A(\hat{\mathbf{r}}) Y_{\ell m}(\hat{\mathbf{r}}) e^{2\pi i \mathbf{u} \cdot \hat{\mathbf{r}}}. \quad (21)$$

It is of course possible to perform these integrals numerically and calculate the visibility covariance matrix without any approximations at all. In this section we see how to obtain the cylindrical approximation from this exact expression.

In previous treatments (e.g., White et al. 1999), the flat-sky limit for a single pointing was taken by approximating the spherical harmonics near the pole of the spherical coordinate system ($\theta = 0$). To obtain the visibility covariance for two different pointings, it is more convenient to place the pointing centers on the equator as in § 3.

Near the equator $z \equiv \cos \theta \simeq \pi/2 - \theta$. Using the recurrence relations for the associated Legendre polynomials (Abramowitz & Stegun 1972; Gradshteyn & Ryzhik 1980), one can show

$$Y_{\ell m}(\phi, z) \rightarrow N_{\ell m} e^{im\phi} \begin{cases} \cos n_{\ell m} z, & \ell - m \text{ even,} \\ -i \sin n_{\ell m} z, & \ell - m \text{ odd,} \end{cases} \quad (22)$$

with

$$n_{\ell m} = \sqrt{\ell(\ell+1) - m^2}, \quad (23)$$

$$N_{\ell m} = (-1)^{(\ell+m)/2} \frac{2^m}{\sqrt{\pi}} \sqrt{\frac{2\ell+1}{4\pi}} \sqrt{\frac{(\ell-m)!}{(\ell+m)!}} \frac{[(\ell+m-1)/2]!}{[(\ell-m)/2]!}, \quad (24)$$

which can also be written

$$N_{\ell m} = (-1)^{(\ell+m)/2} 2^{-\ell} \sqrt{\frac{2\ell+1}{4\pi}} \frac{\sqrt{(\ell+m)!(\ell-m)!}}{[(\ell+m)/2]![(\ell-m)/2]!} \quad (25)$$

by using (Gradshteyn & Ryzhik 1980)

$$\left(n + \frac{1}{2}\right)! = \sqrt{\pi} \frac{(2n+1)!}{2^{2n+1} n!}. \quad (26)$$

In all of these expressions the factorials should be interpreted as Γ functions for noninteger arguments. In the limit when all of the factorial moments are large, we can use the approximation (Abramowitz & Stegun 1972)

$$\ln N! \simeq \left(N + \frac{1}{2}\right) \ln N - N + \text{const} \quad (27)$$

to write the normalization factor as

$$N_{\ell m} \simeq \frac{(-1)^{(\ell+m)/2}}{\pi} \frac{\sqrt{\ell+1/2}}{(\ell^2 - m^2)^{1/4}}. \quad (28)$$

Note that the $Y_{\ell m}$ are eigenfunctions of the two-dimensional Laplacian with eigenvalues $-\ell(\ell+1)$, and the form of $n_{\ell m}$ guarantees that this is preserved in the cylindrical coordinates:

$$\nabla^2 Y_{\ell m} \rightarrow \left(\frac{\partial^2}{\partial \phi^2} + \frac{\partial^2}{\partial z^2}\right) Y_{\ell m} \quad (29)$$

$$= (-m^2 - n_{\ell m}^2) Y_{\ell m} \quad (30)$$

$$= -\ell(\ell+1) Y_{\ell m}, \quad (31)$$

where the arrow indicates the cylindrical coordinate limit.

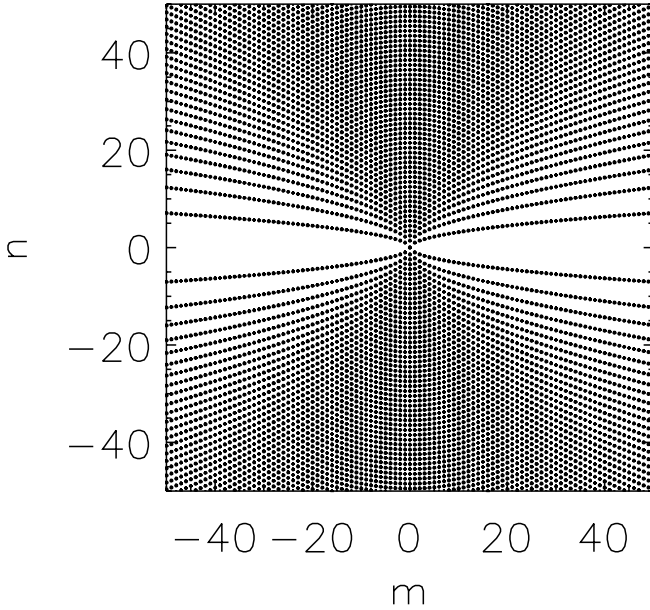


FIG. 4.—Fourier modes $\mathbf{k}_{\ell m}^{\pm} = (m, \pm n_{\ell m})$.

If we define

$$\alpha_{\ell m} = (-1)^{\ell+m} \frac{N_{\ell m}}{2} a_{\ell m}, \quad \bar{\alpha}_{\ell m} = \frac{N_{\ell m}}{2} a_{\ell m}, \quad (32)$$

then we can rewrite equation (18) as

$$T(\boldsymbol{\xi}) = \sum_{\ell m} \alpha_{\ell m} e^{i\mathbf{k} \cdot \boldsymbol{\xi}} + \bar{\alpha}_{\ell m} e^{i\bar{\mathbf{k}} \cdot \boldsymbol{\xi}}, \quad (33)$$

with the definitions $\mathbf{k} = (m, n_{\ell m})$ and $\bar{\mathbf{k}} = (m, -n_{\ell m})$. From now on we take the sum over both $\pm n_{\ell m}$ as implicit and write

$$T(\boldsymbol{\xi}) = \sum_{\mathbf{k}} \alpha_{\mathbf{k}} e^{i\mathbf{k} \cdot \boldsymbol{\xi}}. \quad (34)$$

This way of writing the spherical harmonic expansion makes the correspondence with the Fourier representation explicit.

The visibility becomes

$$V(\mathbf{u}) = (2\pi)^2 \sum_{\mathbf{k}} \alpha(\mathbf{k}) \tilde{A}^*(\mathbf{k} + 2\pi\mathbf{u}), \quad (35)$$

and the correlation matrix is

$$\mathcal{V}_{12} = \frac{(2\pi)^4}{4} \sum_{\mathbf{k}} |N_{\ell m}|^2 C_{\ell} \mathcal{W}_{12}(\mathbf{u}_1, \mathbf{u}_2, \frac{\mathbf{k}}{2\pi}) e^{i\mathbf{k} \cdot \boldsymbol{\beta}}, \quad (36)$$

plus oscillatory terms that average to zero in the sum over ℓ and m . Here $\boldsymbol{\beta}$ is the vector difference between the two pointing centers.

If we work at large values of ℓ and m , we can replace the sum over \mathbf{k} with \sum_m and $\int dn$ and recover our cylindrical result, equation (14). One can verify by explicit computation that using

$$\frac{d\ell}{dn} = \frac{\sqrt{\ell(\ell+1) - m^2}}{\ell + 1/2} \quad (37)$$

to turn the sum over ℓ into an integral and using the asymptotic form of $N_{\ell m}$ in equation (36) leads to equation (14).

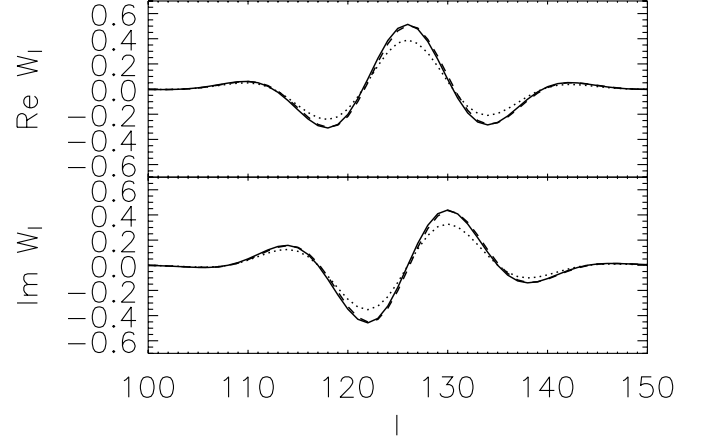


FIG. 5.—Comparison of approximations. The window function is shown for the covariance between visibilities with $\mathbf{u} = 20\hat{\phi}$, beam width $\sigma = 5^\circ$, and pointing centers separated by $\beta = 15^\circ$. The solid curve is the exact spherical harmonic calculation; the dashed curve is the cylindrical approximation; and the dotted curve is the approximation obtained by approximating the spherical harmonics by plane waves.

As Figure 4 illustrates, the differences between the harmonic and Fourier expansions lie in the nonuniform gridding of the wavevectors \mathbf{k} . For any given wavenumber ℓ the modes are packed more sparsely near the m -axis, corresponding to $|m| \simeq \ell$, and more densely near $m \simeq 0$. The normalization factor $N_{\ell m}$ weights the higher m modes more strongly to make up for this.

Surprisingly, in some cases the cylindrical approximation proves numerically more accurate than the approximation in this section, as illustrated in Figure 5. Specifically, in cases where the baseline vectors point in the $\hat{\phi}$ -direction, the sum in equation (36) is dominated by modes with $|m| = \ell$, which are precisely the modes for which the plane-wave approximation to $Y_{\ell m}$ is worst. We found no instance in which the cylindrical approximation (22) does worse than the approximate spherical harmonic expansion of this section, so for numerical work one should use either the cylindrical approximation or the exact full-sky expressions. In general, we find that the cylindrical approximation starts to become poor for Gaussian beam widths $\sigma \simeq 8^\circ$ (FWHM $\simeq 20^\circ$).

5. POLARIZATION

In this section we generalize the results of the previous sections to observations of linear polarization. Instead of considering a single scalar observable T , we must consider observations of the two Stokes parameters Q and U . (The CMB is not expected to be circularly polarized, so we ignore the Stokes parameter V .) Tinbergen (1996) provides a useful introduction to astronomical polarimetry, and Thompson et al. (1994) discusses the formalism of interferometric polarimetry in detail. Bunn (2006) discusses the different systematic error sensitivities of linear and circular polarization experiments in interferometric CMB polarimetry.

It is convenient to combine the Stokes parameters into the complex quantities

$$P_{\pm} = \frac{1}{\sqrt{2}}(Q \pm iU), \quad (38)$$

because these quantities transform in a relatively simple way under rotations; under a rotation by an angle ψ about a given point $\hat{\mathbf{r}}$, $P_{\pm}(\hat{\mathbf{r}}) \rightarrow P_{\pm}(\hat{\mathbf{r}}) e^{\mp 2i\psi}$. In other words, P_+ is a quantity of spin weight -2 and P_- has spin weight $+2$. These transformation properties make (P_+, P_-) a more convenient basis of observables

to work with than (Q, U) . The two bases are related by a unitary transformation,

$$\begin{pmatrix} P_+ \\ P_- \end{pmatrix} = \frac{1}{\sqrt{2}} \begin{pmatrix} 1 & 1 \\ -i & i \end{pmatrix} \begin{pmatrix} Q \\ U \end{pmatrix}, \quad (39)$$

so any results derived in one basis can easily be transformed to the other.

An interferometer that works by interfering circularly polarized radiation from the two antennas measures the visibilities

$$V_{\pm}(\mathbf{u}) = \int d^2\hat{\mathbf{r}} P_{\pm}(\hat{\mathbf{r}}) A(\hat{\mathbf{r}}) e^{2\pi i \mathbf{u} \cdot \hat{\mathbf{r}}}. \quad (40)$$

Specifically, interfering left-circularly polarized radiation from antenna 1 with right-circularly polarized radiation from antenna 2 yields V_+ , and reversing the senses of both circular polarizations yields V_- . (Interfering right with right and left with left yields visibilities that probe total intensity and circular polarization.)

An interferometric polarimeter can also work by combining linear polarization states instead of circular ones. In this case, a visibility V_{xy} obtained by correlating horizontal polarization in one horn with vertical polarization in another probes the combination of Stokes parameters $U + iV$. Averaging V_{xy} and V_{yx} together gives a visibility V_U proportional to Stokes U . A visibility that probes Stokes Q can be obtained by measuring linear polarization states that are oriented at 45° from the x - and y -directions.² We assume that the measured³ quantities are V_{\pm} rather than V_{QU} , but all results are easily transformed to the Q, U basis using equation (39).

As in the case of temperature anisotropy, the key ingredient in analyzing CMB interferometric observations of polarization is the visibility covariance matrix:

$$\mathcal{V}_{12}^{\pm\pm} \equiv \langle V_{\pm}(\mathbf{u}_1, \mathcal{P}_1) V_{\pm}(\mathbf{u}_2, \mathcal{P}_2)^* \rangle, \quad (41)$$

where \mathbf{u}_i and \mathcal{P}_i represent baselines and pointing centers for a pair of visibilities. Note that in this equation the two signs \pm can be varied independently; that is, there are in general four distinct covariances, \mathcal{V}_{12}^{++} , \mathcal{V}_{12}^{+-} , \mathcal{V}_{12}^{-+} , and \mathcal{V}_{12}^{--} .

Our primary interest continues to be the case in which the flat-sky approximation is appropriate for each individual pointing, but the separation between pointings is not necessarily small. We present the flat-sky approximation first, followed by exact expressions for the visibility covariances in terms of spherical harmonics. We then show that the spherical harmonic expressions reduce in this limit to cylindrical-sky expressions similar to the anisotropy results above.

5.1. Flat Sky

Assume our observations cover a small enough patch of sky that we can replace spherical harmonic expansions with Fourier transforms:

$$P_{\pm}(\mathbf{x}) = \int d^2\mathbf{k} \tilde{P}_{\pm}(\mathbf{k}) e^{i\mathbf{k} \cdot \mathbf{x}}. \quad (42)$$

² In principle, Stokes Q can also be measured from the visibilities V_{xx} and V_{yy} , which probe the combinations $I \pm Q$. In practice, however, since $I \gg Q$ for CMB polarization, this is an inferior way to probe Q .

³ We are ignoring some sources of systematic error in this expression. For instance, in an instrument with cross-polar beam response, each measured visibility would contain contributions from both P_+ and P_- , with different effective antenna patterns.

The two Fourier transforms satisfy the relation

$$\tilde{P}_{\pm}^*(\mathbf{k}) = \tilde{P}_{\mp}(-\mathbf{k}). \quad (43)$$

A key insight into the analysis of CMB polarization was the observation (Kamionkowski et al. 1997; Zaldarriaga & Seljak 1997) that any polarization field can be decomposed into a scalar part (conventionally denoted E) and a pseudoscalar part (denoted B). The E - B separation is particularly simple in Fourier space; modes with polarization parallel or perpendicular to \mathbf{k} are E modes, while modes polarized at 45° are B modes. In terms of \tilde{P}_{\pm} , this means that

$$\tilde{P}_{\pm}(\mathbf{k}) = [\tilde{E}(\mathbf{k}) \pm i\tilde{B}(\mathbf{k})] e^{\pm 2i\psi_{\mathbf{k}}}, \quad (44)$$

where $\psi_{\mathbf{k}}$ is the angle made by the wavevector \mathbf{k} with respect to the x -axis.

Assuming that the polarization was generated by a homogeneous, isotropic, parity-respecting process, the two-point correlations between E and B are determined by two power spectra \mathcal{P}_E and \mathcal{P}_B :

$$\langle \tilde{E}(\mathbf{k}) \tilde{E}^*(\mathbf{k}') \rangle = (2\pi)^{-2} \mathcal{P}_E(k) \delta(\mathbf{k} - \mathbf{k}'), \quad (45)$$

$$\langle \tilde{B}(\mathbf{k}) \tilde{B}^*(\mathbf{k}') \rangle = (2\pi)^{-2} \mathcal{P}_B(k) \delta(\mathbf{k} - \mathbf{k}'), \quad (46)$$

$$\langle \tilde{E}(\mathbf{k}) \tilde{B}^*(\mathbf{k}') \rangle = 0. \quad (47)$$

This means that the covariances of the polarization \tilde{P}_{\pm} are

$$\langle \tilde{P}_{\pm}(\mathbf{k}) \tilde{P}_{\pm}^*(\mathbf{k}') \rangle = (2\pi)^{-2} [\mathcal{P}_E(k) + \mathcal{P}_B(k)] \delta(\mathbf{k} - \mathbf{k}'), \quad (48)$$

$$\langle \tilde{P}_{\pm}(\mathbf{k}) \tilde{P}_{\mp}^*(\mathbf{k}') \rangle = (2\pi)^{-2} [\mathcal{P}_E(k) - \mathcal{P}_B(k)] e^{\pm 4i\psi_{\mathbf{k}}} \delta(\mathbf{k} - \mathbf{k}'). \quad (49)$$

Just as in the scalar case, the visibility associated with a pointing center \mathbf{b} and a baseline \mathbf{u} can be expressed in terms of the Fourier transform of the antenna pattern:

$$V_{\pm}(\mathbf{u}, \mathbf{b}) = (2\pi)^2 \int d^2\mathbf{k} \tilde{A}^*(\mathbf{k} + 2\pi\mathbf{u}) \tilde{P}_{\pm}(\mathbf{k}) e^{i\mathbf{k} \cdot \mathbf{b}}. \quad (50)$$

The correlation between two visibilities is

$$\mathcal{V}_{12}^{\pm\pm} = (2\pi)^2 \int \left\{ d^2\mathbf{k} \tilde{A}^*(\mathbf{k} + 2\pi\mathbf{u}_1) \tilde{A}(\mathbf{k} + 2\pi\mathbf{u}_2) \times e^{i\mathbf{k} \cdot (\mathbf{b}_1 - \mathbf{b}_2)} [\mathcal{P}_E(k) + \mathcal{P}_B(k)] \right\}, \quad (51)$$

$$\mathcal{V}_{12}^{\pm\mp} = (2\pi)^2 \int \left\{ d^2\mathbf{k} \tilde{A}^*(\mathbf{k} + 2\pi\mathbf{u}_1) \tilde{A}(\mathbf{k} + 2\pi\mathbf{u}_2) \times e^{i\mathbf{k} \cdot (\mathbf{b}_1 - \mathbf{b}_2)} [\mathcal{P}_E(k) - \mathcal{P}_B(k)] e^{\pm 4i\psi_{\mathbf{k}}} \right\}. \quad (52)$$

5.2. Spherical Harmonics

Since the quantities P_{\pm} are quantities of spin weight ∓ 2 , it is natural to expand them in spin (± 2) spherical harmonics:

$$P_{\pm}(\hat{\mathbf{r}}) = \sum_{\ell, m} a_{\mp 2, \ell m} Y_{\ell m}(\hat{\mathbf{r}}). \quad (53)$$

The decomposition into E and B components is particularly simple in terms of the spherical harmonic coefficients:

$$a_{\pm 2, \ell m} = E_{\ell m} \pm iB_{\ell m}. \quad (54)$$

The two-point statistics are completely described by two power spectra C_ℓ^{EE} and C_ℓ^{BB} :

$$\langle E_{\ell m} E_{\ell' m'}^* \rangle = C_\ell^{EE} \delta_{\ell\ell'} \delta_{mm'}, \quad (55)$$

$$\langle B_{\ell m} B_{\ell' m'}^* \rangle = C_\ell^{BB} \delta_{\ell\ell'} \delta_{mm'}, \quad (56)$$

$$\langle E_{\ell m} B_{\ell' m'}^* \rangle = 0. \quad (57)$$

As in the case of temperature anisotropy, the spherical and flat-sky power spectra are related via $C_\ell \simeq \mathcal{P}(u)$ with $l = 2\pi u$.

The visibilities can be expressed in terms of the spherical harmonic coefficients as

$$V_\pm(\mathbf{u}) = \sum_{\ell, m} a_{\mp 2, \ell m} F_{\mp 2, \ell m}(\mathbf{u}), \quad (58)$$

where

$$F_{\mp 2, \ell m}(\mathbf{u}) = \int d^2\hat{\mathbf{r}} A(\hat{\mathbf{r}}) {}_{\mp 2}Y_{\ell m}(\hat{\mathbf{r}}) e^{2\pi i \mathbf{u} \cdot \hat{\mathbf{r}}}. \quad (59)$$

Consider first the covariance between two visibilities with identical pointing centers. Combining equations (41) and (54)–(58), the visibility covariances can be shown to be

$$\mathcal{V}_{12}^{\pm\pm} = \sum_{\ell} (C_\ell^E + C_\ell^B) W_\ell^{\pm\pm}, \quad (60)$$

$$\mathcal{V}_{12}^{\pm\mp} = \sum_{\ell} (C_\ell^E - C_\ell^B) W_\ell^{\pm\mp}, \quad (61)$$

where

$$W_\ell^{\pm\pm} = \sum_m F_{\mp 2, \ell m}(\mathbf{u}_1) F_{\mp 2, \ell m}^*(\mathbf{u}_2). \quad (62)$$

In the case where the two observations have different pointing centers, we once again transform to a coordinate system with both pointing centers on the equator, separated by an angle β . Because the spin-weighted spherical harmonics have azimuthal dependence $e^{im\phi}$, the only change is an additional factor of $e^{im\beta}$:

$$W_\ell^{\pm\pm} = \sum_m e^{im\beta} F_{\mp 2, \ell m}(\mathbf{u}_1) F_{\mp 2, \ell m}^*(\mathbf{u}_2). \quad (63)$$

In order to calculate the correlation between a pair of observations with arbitrary pointing centers, we simply rotate to a new coordinate system that places both centers on the equator before applying the above results. In performing this rotation, it is important to remember to transform P_\pm (and hence V_\pm) by $e^{\pm 2i\delta}$, where δ is the angle through which the polarization basis directions are rotated by the transformation. To be specific, if the change of coordinates results in a rotation of the $\hat{\theta}$ - and $\hat{\phi}$ -directions at each of the pointing centers by δ_1 and δ_2 , then $\mathcal{V}_{12}^{\pm\pm} \rightarrow \mathcal{V}_{12}^{\pm\pm} e^{2i(\pm\delta_1 \mp \delta_2)}$. See the Appendix for an explicit recipe for finding these angles.

5.3. Connecting Flat-Sky to Spherical

As in the case of temperature anisotropy, we can see the connection between the spherical and flat-sky calculations of polarization by considering observations that lie near the equator of our spherical coordinate system and approximating the sphere by a cylinder. By applying the spin-raising operator (e.g., Lewis

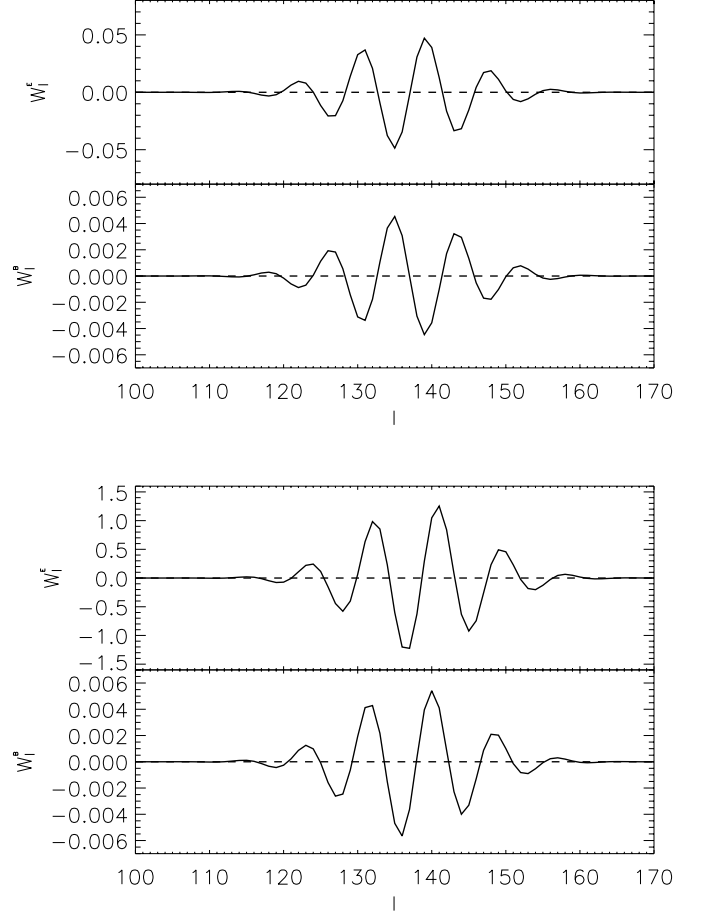


FIG. 6.—Polarization window functions. *Top*: Window functions for the correlation $\langle V_Q V_Q^* \rangle$ of the two baselines at the upper corners of Fig. 2. *Bottom*: Correlations calculated by incorrectly assuming that the entire mosaic is flat, that is, ignoring the rotation of the basis vectors $\hat{\theta}$ and $\hat{\phi}$ when moving from one point to another. Note that the vertical axes of the two W_l^E plots differ by a factor of 200. These window functions were calculated in the cylindrical approximation, but the exact spherical harmonic calculation yields negligible differences.

et al. 2002) to the plane-wave approximation to the spherical harmonics (22), one can show that in this limit

$${}_2Y_{lm}(\hat{\mathbf{r}}) = N_{lm}^{(2)} e^{im\phi} \begin{cases} \cos(n_{lm}z + \delta_{lm}), & l - m \text{ even,} \\ -i \sin(n_{lm}z + \delta_{lm}), & l - m \text{ odd,} \end{cases} \quad (64)$$

with

$$N_{lm}^{(2)} = N_{lm} l(l+1) \sqrt{\frac{(l-2)!}{(l+2)!}} = N_{lm} \sqrt{\frac{l(l+1)}{(l+2)(l-1)}}, \quad (65)$$

$$\delta_{lm} = 2 \cos^{-1} \frac{m}{l(l+1)}. \quad (66)$$

By reasoning similar to that in § 4, we can use this to connect the spherical harmonic formalism to the flat-sky limit.

5.4. Example

Consider a 10×10 mosaic of pointings of an interferometer, with the same parameters as in the example of § 3: the Gaussian beam width is $\sigma = 5^\circ$, and the pointings are centered on the equator and separated by 5° in both θ and ϕ . We consider only one baseline per pointing, with $\mathbf{u} = 22\hat{\phi}$. Assume that both visibilities V_Q and V_U are measured (either directly or by measuring V_\pm).

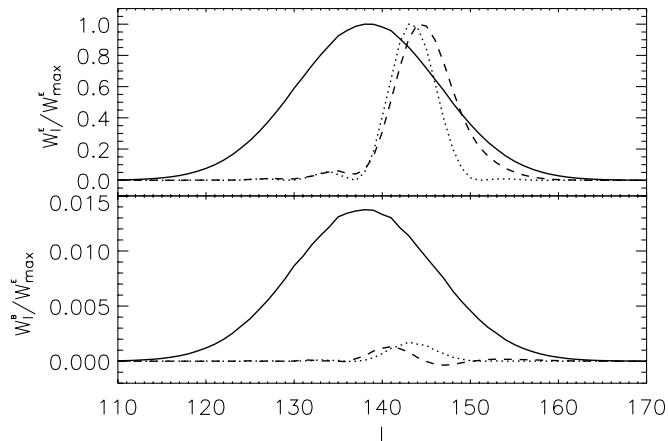


FIG. 7.—Window functions for a single pointing (*solid curve*), the sum of all pointings (*dashed curve*), and the sum of all pointings neglecting sky curvature (*dotted curve*).

For any pair of pointings we can define E and B window functions such that

$$\langle V_{Qi} V_{Qj}^* \rangle = \sum_{\ell} (W_{\ell}^E C_{\ell}^{EE} + W_{\ell}^B C_{\ell}^{BB}), \quad (67)$$

where V_{Qi} is the visibility for Stokes Q corresponding to baseline i . In the limit of infinitely sharp ℓ -space resolution, we would expect W_{ℓ}^B to vanish, since the polarization would be parallel to the baseline \mathbf{u} . Inevitably, however, when only part of the sky is covered (leading to imperfect Fourier-space resolution), there is some mixing of E and B modes (Lewis et al. 2002; Bunn 2002; Bunn et al. 2003).

For the case of the two visibilities at the upper corners of the grid, these window functions are shown in Figure 6. As in the scalar case, the correlations are strongly affected by the rotation of the coordinate basis. If we incorrectly model the entire mosaic as flat, treating the basis vectors $\hat{\theta}$ and $\hat{\phi}$ at each point to be parallel, the correlation between these two pointings would be dramatically overestimated. In fact, by treating the sky as flat, we would be making two separate errors: treating the two baseline vectors as parallel (just as in the case of temperature anisotropy in § 3) and failing to apply the appropriate transformation to the Stokes parameters (Q, U).

Figure 7 illustrates the improvement of resolution due to mosaicking in this example. Like Figure 3, this figure shows the autocorrelation window function for a single pointing, as well as that of the sum of all 100 pointings in the grid. If we neglect sky curvature, we overestimate the correlation between distant baselines and hence also overestimate the improvement in ℓ -space resolution.

6. CONCLUSIONS

Interferometers have been used to great effect in measuring CMB temperature and polarization anisotropies. The formalism for analyzing interferometer data, however, has only been fully developed in the small-field-of-view or flat-sky limit. Future experiments that aim for exquisite ℓ -space resolution will need to survey large areas of sky outside the realm of validity of the existing formalism.

In this paper we have extended the formalism to the situation where we can approximate the sky as flat for each individual pointing of the instrument, but we relax the assumption that the angle between pointings is also small. We have connected the full-sky spherical harmonic approach to the flat-sky Fourier approach in two distinct ways and derived approximations for the visibility covariance matrix in each. We find that the cylindrical method of § 3 and § 5.2 works better in all cases than the harmonic method of § 4 and provides accurate approximations to the full-sky expressions for individual pointings smaller than 20° FWHM. Mosaicking together many pointings increases the ℓ -space resolution, but in the cases considered here the improvement is less than would be predicted from the flat-sky formalism, in large part due to the effects of baseline rotation. If we neglect sky curvature we overestimate the correlation between distant baselines and hence also overestimate the improvement in ℓ -space resolution.

E. F. B. is supported by NSF grant AST 05-07395 and a Cottrell Award from the Research Corporation. E. F. B. thanks the physics departments of Brown University and MIT for their hospitality during the completion of this work. M. W. is supported by NASA. We thank Asantha Cooray and Manoj Kaplinghat, the organizers of the March 2006 workshop on Fundamental Physics with Cosmic Microwave Background Radiation, where this work was initiated.

APPENDIX

In calculating the covariance between visibilities at two different pointing centers \hat{r}_1 and \hat{r}_2 , we must transform to a coordinate system that places both pointing centers on the equator. This affects both the components of the baseline vectors \mathbf{u}_1 and \mathbf{u}_2 and (in the case of polarization) the Stokes parameters Q and U . We present here an explicit recipe for performing this transformation.

Throughout this appendix, unprimed symbols refer to the original coordinate system, and primed symbols refer to a coordinate system (x', y', z') such that \hat{r}_1 lies on the x' -axis and \hat{r}_2 is in the x' - y' plane. First, choose the z' -axis to be perpendicular to both vectors:

$$\hat{z}' = \frac{\hat{r}_1 \times \hat{r}_2}{|\hat{r}_1 \times \hat{r}_2|}. \quad (A1)$$

Next, choose the y' -axis to be perpendicular to both \hat{z}' and \hat{r}_1 :

$$\hat{y}' = \hat{r}_1 \times \hat{z}'. \quad (A2)$$

Finally, choose $\hat{x}' = \hat{y}' \times \hat{z}'$. In spherical coordinates (θ', ϕ') defined with respect to the primed coordinate system, we have $\hat{r}_1 = (\pi/2, 0)$ and $\hat{r}_2 = (\pi/2, \beta)$ with β such that $(\cos \beta, \sin \beta) = (\hat{r}_2 \cdot \hat{x}', \hat{r}_2 \cdot \hat{y}')$.

Say that the baseline vector \mathbf{u}_i ($i = 1, 2$) is expressed in the original (unrotated) spherical coordinate system as

$$\mathbf{u}_i = u_{i\theta}\hat{\boldsymbol{\theta}} + u_{i\phi}\hat{\boldsymbol{\phi}}. \quad (\text{A3})$$

We need to know the corresponding components in the rotated coordinate system. The components of the basis vectors $\hat{\boldsymbol{\theta}}$ and $\hat{\boldsymbol{\phi}}$ in the rotated coordinate system are

$$\hat{\boldsymbol{\theta}} = (\cos \delta_i)\hat{\boldsymbol{\theta}}' - (\sin \delta_i)\hat{\boldsymbol{\phi}}', \quad (\text{A4})$$

$$\hat{\boldsymbol{\phi}} = (\sin \delta_i)\hat{\boldsymbol{\theta}}' + (\cos \delta_i)\hat{\boldsymbol{\phi}}'. \quad (\text{A5})$$

The easiest way to find the rotation angle δ_i is to compute the components of $\hat{\boldsymbol{\phi}} = (\hat{\mathbf{z}} \times \hat{\mathbf{r}}_i)/|\hat{\mathbf{z}} \times \hat{\mathbf{r}}_i|$ and take the dot product $\sin \delta_i = \hat{\boldsymbol{\phi}} \cdot \hat{\boldsymbol{\theta}}' = \hat{\boldsymbol{\phi}} \cdot (-\hat{\mathbf{z}}')$, since $\hat{\mathbf{r}}_i$ is on the equator in the primed coordinate system.

Once the rotation angles δ_1 and δ_2 are known, the components of the baseline vectors are

$$\begin{pmatrix} u_{i\theta'} \\ u_{i\phi'} \end{pmatrix} = \begin{pmatrix} \cos \delta_i & \sin \delta_i \\ -\sin \delta_i & \cos \delta_i \end{pmatrix} \cdot \begin{pmatrix} u_{i\theta} \\ u_{i\phi} \end{pmatrix}. \quad (\text{A6})$$

In calculating the polarization visibilities we replace (Q, U) with

$$\begin{pmatrix} Q' \\ U' \end{pmatrix} = \begin{pmatrix} \cos 2\delta_i & \sin 2\delta_i \\ -\sin 2\delta_i & \cos 2\delta_i \end{pmatrix} \cdot \begin{pmatrix} Q \\ U \end{pmatrix}. \quad (\text{A7})$$

REFERENCES

- Abramowitz, M., & Stegun, I. A. 1972, Handbook of Mathematical Functions (New York: Dover)
- Baker, J. C., et al. 1999, MNRAS, 308, 1173
- Bunn, E. F. 2002, Phys. Rev. D, 65, 3003 (erratum 66, 069902)
- . 2006, Phys. Rev. D, submitted (astro-ph/0607312)
- Bunn, E. F., Zaldarriaga, M., Tegmark, M., & de Oliveira-Costa, A. 2003, Phys. Rev. D, 67, 3501
- Cornwell, T. J. 1988, A&A, 202, 316
- Cornwell, T. J., Holdaway, M. A., & Uson, J. M. 1993, A&A, 271, 697
- Ekers, R. D., & Rots, A. H. 1979, in IAU Colloq. 49, Image Formation from Coherence Functions in Astronomy, ed. C. van Schooneveld (Dordrecht: Reidel), 61
- Gradshteyn, I. S., & Ryzhik, I. M. 1980, Table of Integrals, Series and Products (San Diego: Academic)
- Halverson, N. W., et al. 2002, ApJ, 568, 38
- Hobson, M. P., Lasenby, A. N., & Jones, M. 1995, MNRAS, 275, 863
- Hobson, M. P., & Magueijo, J. 1996, MNRAS, 283, 1133
- Hobson, M. P., & Maisinger, K. 2002, MNRAS, 334, 569
- Holdaway, M. A. 1999, in ASP Conf. Ser. 180, Synthesis Imaging in Radio Astronomy II, ed. G. B. Taylor, C. L. Carilli, & R. A. Perley (San Francisco: ASP), 401
- Kamionkowski, M., Kosowsky, A., & Stebbins, A. 1997, Phys. Rev. D, 55, 7368
- Leitch, E. M., et al. 2005, ApJ, 624, 10
- Lewis, A., Challinor, A., & Turok, N. 2002, Phys. Rev. D, 65, 3505
- Martin, H. M., & Partridge, R. B. 1988, ApJ, 324, 794
- Myers, S. T., et al. 2003, ApJ, 591, 575
- O'Sullivan, C., et al. 1995, MNRAS, 274, 861
- Park, C.-G., & Ng, K.-W. 2004, ApJ, 609, 15
- Park, C.-G., Ng, K.-W., Park, C., Liu, G.-C., & Umetsu, K. 2003, ApJ, 589, 67
- Pearson, T. J., et al. 2003, ApJ, 591, 556
- Readhead, A. C. S., et al. 2004, Science, 306, 836
- Subrahmanyan, R., Ekers, R. D., Sinclair, M., & Silk, J. 1993, MNRAS, 263, 416
- Taylor, A. C., et al. 2003, MNRAS, 341, 1066
- Thompson, A. R., Moran, J. M., & Swenson, G. W. 1994, Interferometry and Synthesis in Radio Astronomy (Malabar: Krieger)
- Tinbergen, J. 1996, Astronomical Polarimetry (Cambridge: Cambridge Univ. Press)
- White, M., Carlstrom, J. E., Dragovan, M., & Holzzapfel, S. W. L. 1999, ApJ, 514, 12
- Zaldarriaga, M., & Seljak, U. 1997, Phys. Rev. D, 55, 1830